PNAS RESEARCH ARTICLE | NEUROSCIENCE

Role of intracortical neuropil growth in the gyrification of the primate cerebral cortex

Brian G. Rash[a,1], Jon I. Arellano[a], Alvaro Duque[a], and Pasko Rakic[a,b,2]

Edited by David Van Essen, Washington University in St. Louis School of Medicine, St. Louis, MO; received July 21, 2022; accepted November 10, 2022

The convolutions of the mammalian cerebral cortex allow the enlargement of its surface and addition of novel functional areas during evolution while minimizing expansion of the cranium. Cognitive neurodevelopmental disorders in humans, including microcephaly and lissencephaly, are often associated with impaired gyrification. In the classical model of gyrification, surface area is initially set by the number of radial units, and the forces driving cortical folding include neuronal growth, formation of neuropil, glial cell intercalation, and the patterned growth of subcortical white matter. An alternative model proposes that specified neurogenic hotspots in the outer subventricular zone (oSVZ) produce larger numbers of neurons that generate convexities in the cortex. This directly contradicts reports showing that cortical neurogenesis and settling of neurons into the cortical plate in primates, including humans, are completed well prior to the formation of secondary and tertiary gyri and indeed most primary gyri. In addition, during the main period of gyrification, the oSVZ produces mainly astrocytes and oligodendrocytes. Here we describe how rapid growth of intracortical neuropil, addition of glial cells, and enlargement of subcortical white matter in primates are the primary forces responsible for the post-neurogenic expansion of the cortical surface and formation of gyri during fetal development. Using immunohistochemistry for markers of proliferation and glial and neuronal progenitors combined with transcriptomic analysis, we show that neurogenesis in the ventricular zone and oSVZ is phased out and transitions to gliogenesis prior to gyral development. In summary, our data support the classical model of gyrification and provide insight into the pathogenesis of congenital cortical malformations.

gyrification | cortex | neurogenesis

A highly convoluted cerebrum is typical of large mammals including humans, and generations of scientists have wondered at how such a complex morphological configuration arose. The extraordinary expansion of the cerebral cortex and acquisition of new functional areas during mammalian evolution is primarily due to the expansion of the neurogenic proliferative niche in the ventricular zone (VZ) near the lateral ventricles (1–5). This is in essence a modular process, via the addition of radial units, that will increase the number of cortical columns and the surface area of the cortex.

At the turn of the millennium, there was general consensus that gyrification is driven by a variety of mechanical factors (3, 6–8). However, the precise forces explaining the specific patterns of gyri and sulci that are reproducible between individuals of a given species were a matter of debate. There were three main ideas: one described by Richman (9) proposing that differential growth of upper layers versus lower layers in the cortical plate generates lateral tension that is released through buckling of the cortex. Another hypothesis, proposed by Van Essen (10), involved axon tension between connected cortical areas that would fold the cortical surface. A third hypothesis involved a variety of cellular growth processes that combined to amplify cortical surface area, including 1) increased neuronal cell body size and growth of dendritic arbors, 2) the ingrowth of intracortical axons and elaboration of dendritic spines with synaptic connections, 3) intercalation and growth of subcortically derived interneurons and glial cells, and 4) formation and growth of blood vessels (6, 11). In addition, other possible contributors to gyrification were described, including the ratio of subplate and cortical thickness or the size and shape of subcortical axon bundles, as well as the surgical manipulation of such axonal connections, which had profound impacts on gyral size and pattern (11, 12).

In the last decade, a new hypothesis has emerged, positing that regionally defined "hot spots" of neurogenesis in the outer subventricular zone (oSVZ) define the location of each prospective gyrus. Expanding on the Richman model (9) of differential growth of cortical layers, this hypothesis proposes that those hot spots in the oSVZ produce a locally greater number of neurons destined to the superficial cortical layers that, upon their arrival in the cortical plate, induce an arc-shaped surface convexity (13–17) that will become a gyrus. This hypothesis has been disputed, mostly based on the fact that

Significance

The convolutions of the mammalian cortex allow the enlargement of its surface and addition of novel functional areas during evolution while minimizing expansion of the cranium. Cognitive neurodevelopmental disorders in humans, including microcephaly and lissencephaly, are often associated with impaired gyral development. Here we describe that rapid, post-neurogenic neuropil growth, addition of glial cells, and enlargement of subcortical white matter in primates are responsible for much of the cortical surface area expansion during fetal development and are primary driving forces for the subsequent process of gyrification. Our study clarifies the mechanisms determining how brain convolutions form and provides a fundamental conceptual framework and insight into pathogenesis of a variety of cortical malformations and associated cognitive impairments.

Author contributions: B.G.R. and P.R. designed research; B.G.R. performed research; A.D. contributed new reagents/analytic tools; B.G.R., J.I.A., and P.R. analyzed data; A.D. organized and provided macaque tissue for analysis; P.R. supervised the project; and B.G.R. J.I.A., A.D., and P.R. wrote the paper.

The authors declare no competing interest.

This article is a PNAS Direct Submission.

[1]Present address: Herophilus, Inc., San Francisco, CA 94107.

[2]To whom correspondence may be addressed. Email: pasko.rakic@yale.edu.

This article contains supporting information online at https://www.pnas.org/lookup/suppl/doi:10.1073/pnas.2210967120/-/DCSupplemental.

Published December 27, 2022.

neurogenesis is basically over by the time gyrification starts (18–22). However, in spite of this, the concept of neurogenic induction of gyrification has gained support in recent years. Since detailed studies of the timing of cortical neurogenesis in the macaque monkey have been reported, we have here used the macaque cerebrum as a model to reassess the fundamental principles of primate gyrification.

Results

We examined 21 macaque brains at multiple developmental stages between embryonic day (E) 55 and 3 y of age, to assess the progression of cortical gyrification in relation to neurogenesis and cortical plate formation. At E90, when neurogenesis is basically completed in most cortical regions, the frontal cortical plate remains almost completely lissencephalic, but by E138, deep sulci have appeared, demarcating all of the major primary gyri (Fig. 1). The timing of gyrification in the macaque monkey has been extensively described (23–29), showing that the first indentation to appear in the cortical surface is the Sylvian fissure (SF) at about E75. However, the SF is not a neocortical sulcus, but rather a fissure like the interhemispheric fissure that has clear mechanical origins which have been previously characterized (6, 7, 30). Then, around E80, the calcarine sulcus begins to form in the occipital cortex (Table 1) (24). Apart from those early invaginations, the brain is almost entirely lissencephalic at E90, and by E97, the brain shows only shallow grooves where a few prospective gyri are starting to form, such as those created by the appearance of the central and superior temporal sulci (Table 1 and Fig. 2 *A*, *Inset*) (25). By E90, the excitatory neurons for most cortical regions have been already produced: excitatory neurogenesis is complete by E70 in the cingulate cortex (Brodmann area 24); by E80 in prefrontal area 11 and by E90 in prefrontal area 46; only the primary visual cortex area 17 shows a protracted neurogenesis period ending around E100 or shortly thereafter (31–33), likely related to the exceptionally large number of excitatory neurons in this

Table 1. List of cerebral sulci present or absent at the end of excitatory neurogenesis at E97. Although some are just beginning to form, these continue to develop and deepen for several months into postnatal life.

Sulci at earliest stages at E97:	Arcuate sulcus
	Cingulate sulcus
	Lunate sulcus
	Intraparietal sulcus
	Superior temporal sulcus
	Calcarine sulcus
Sulci that begin to form after E97:	Principal sulcus
	Central sulcus
	Ectocalcarine sulcus
	Superior precentral dimple
	Arcuate sulcus spur
	Anterior subcentral dimple
	Anterior middle temporal sulcus
	Occipital temporal sulcus
	Circular sulcus
	Superior calcarine sulcus
	Superior postcentral dimple
	Infraprincipal dimple
	Post supraprincipal dimple
	Rostral sulcus
	Medial orbital sulcus
	Lateral orbital sulcus
	Anterior supraprincipal dimple
	Parieto-occipital sulcus

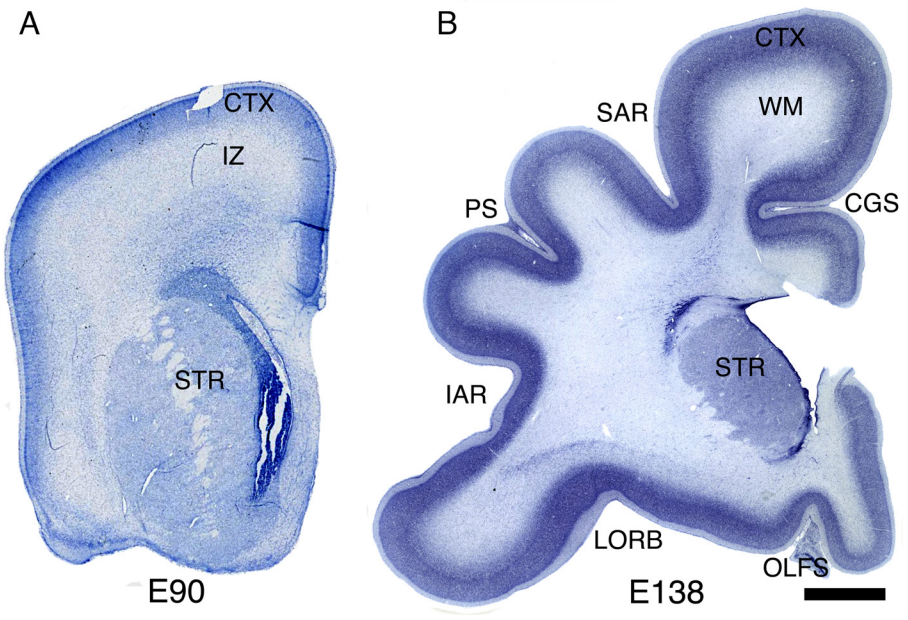

Fig. 1. Rapid cortical surface area growth and gyrification after the completion of excitatory neurogenesis. (*A* and *B*) Coronal sections of macaque frontal cerebrum at E90 and E138 stained for Nissl. Abbreviations: CTX, cerebral cortex; IZ, intermediate zone; WM, white matter; CGS, cingulate sulcus; SAR, superior arcuate sulcus; STR, striatum; PS, principal sulcus; IAR, inferior arcuate sulcus; LORB, lateral orbital sulcus; OLFS, olfactory sulcus. (Scale bar, 2 mm.)

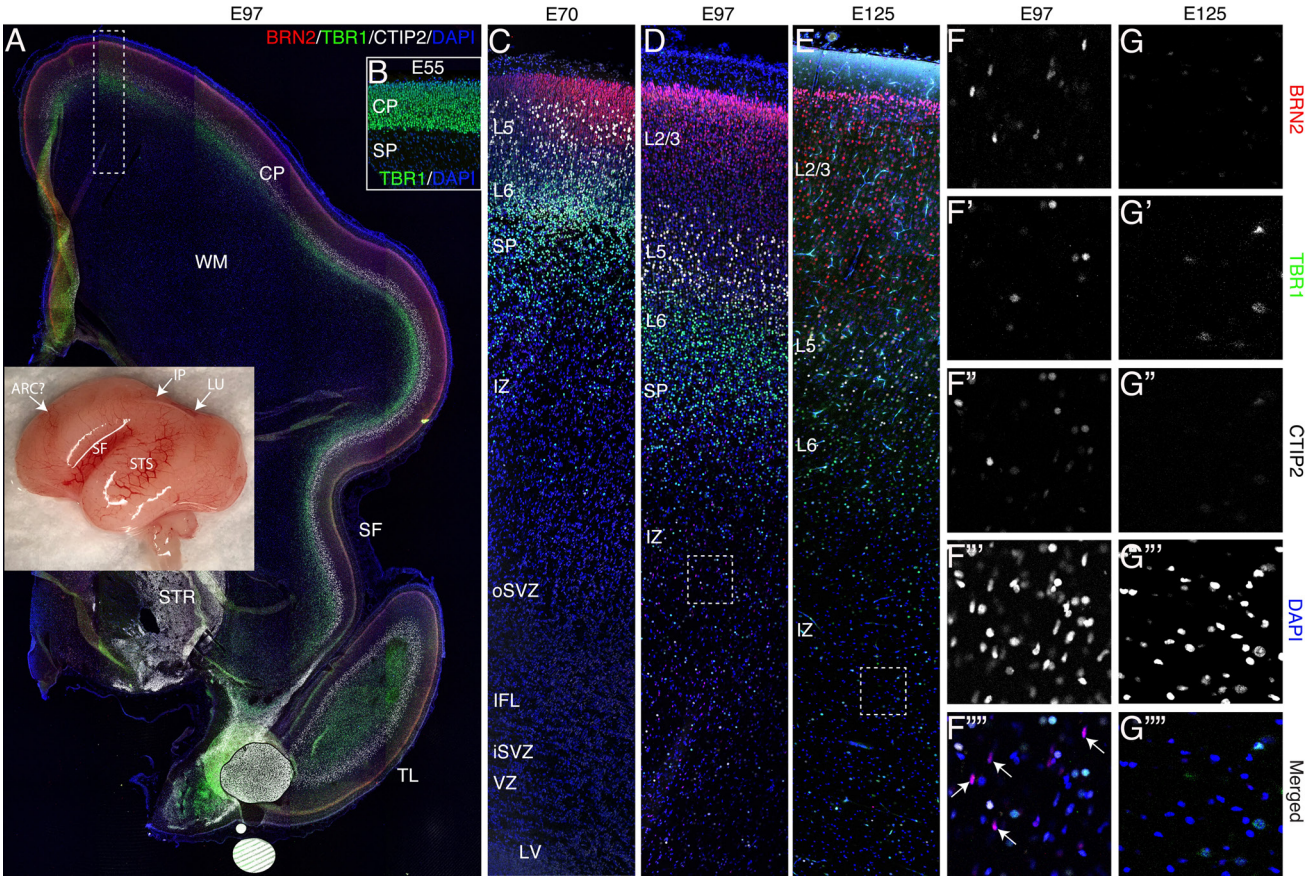

Fig. 2. Development of the cortical plate in macaque from E55 to E125. (*A*) Whole brain (*Inset*) and panoramic view of E97 caudo-frontal cortex in coronal section stained by immunohistochemistry for the cortical layer markers, Brn2 (red; layer 2/3), Ctip2 (white; layer 5), and Tbr1 (green; layer 6/SP). (*B–E*) Time series of high magnification images of dorsal caudo-frontal cortex at the indicated ages; (*D*) corresponds to the boxed region in (*A*). (*F* and *G*) High magnification views of boxed regions in (*D*) and (*E*), respectively. The excitatory neurons of the cortex are almost finished migrating by E97, when a few remaining Brn2+ cells were observed still migrating through the IZ/SP (*D*, *F*, arrows in *F''''*). However, such cells were not found at E125 (*E* and *G*). Position of future SF and superior temporal sulcus demarcating prospective cerebral lobes are indicated (*A*, *Inset*). Abbreviations: ARC, arcuate sulcus; SF, Sylvian fissure; STS, superior temporal sulcus; IP, intraparietal sulcus; LU, lunate sulcus; TL, temporal lobe; CP, cortical plate; WM, white matter; IFL, inner fiber layer. *A–E* represent confocal montages.

region. Therefore, gyrification starts when neurogenesis is already complete, between E90 and E100, and progresses until most neocortical sulci achieve adult dimensions around 3 mo after birth (27) (Fig. 4*B*).

We examined the developing cortex at dorsal frontal and parietal levels at E55, E70, E92, E97, and E125 using layer-specific markers, including Tbr1 (L6 and SP), Ctip2 (BCL11B; L5), and Brn2 (POU3F2; L2/3) by immunohistochemistry (Fig. 2 *A–E*). We found that almost all excitatory cortical neurons were in place around E97, soon after conclusion of neurogenesis in most of the brain. At that age, upper cortical layers were well populated, and only a few remaining Brn2+ upper layer neurons with migratory morphology could be seen traveling through the intermediate zone (IZ) and SP (Fig. 2 *D* and *F''''*), suggesting that excitatory neurogenesis and migration are essentially complete at this age. Most cortical gyri and sulci successively form only after E97 (Table 1 and Fig. 3*B*). At E97 age, there was very little regional variation in thickness of the cortical plate or individual laminae (Fig. 2*A*), and we did not find, in any brain between E55 and E97, variations in thickness associated with future gyral and sulcal locations (N = 8). Our data therefore support the idea that heterogeneities in layer thickness, such as the thinning of deep layers at sulcal fundi that is evident in the mature brain (Fig. 1*B*), are due to secondary distortion due to the mechanical stresses of the folding process itself, as previously suggested (6, 10), and not due to differential neurogenesis with respect to sulci and gyri.

In addition, we found that Tbr2 expression (a specific marker of cortical excitatory intermediate neuronal precursors; INPs) (35, 36) is robust in the inner subventricular zone (iSVZ and oSVZ) at E70, when upper layer neurons are being generated in most cortical regions. However, about 2 wk later, between E92 and E97, very few INPs were found, and they expressed very low levels of Tbr2 compared with E70 (Fig. 3 *B–E*, *H*, and *I*). Consistent with a lack of neurogenesis past E90-100, no Tbr2+ cells could be detected at E125 or E145 (Fig. 3 *D* and *E*), when the development of gyri and sulci is proceeding rapidly. Moreover, transcriptional analysis via the Psychencode project (34) available for E60, E80, and E110 confirmed that Tbr2 expression decreases dramatically to near adult levels by E110 in most cortical regions, supporting the view that cortical excitatory neurogenesis does not continue during the period of gyrification (Fig. 3*A*). Also, data from the NIH Blueprint NHP Atlas https://www.blueprintnhpatlas.org/static/referencedata show that Tbr2 mRNA shows a clear decrease between E80 and E90 and virtual lack of expression at E120 in the VZ, iSVZ and oSVZ of the macaque cingulate cortex. Furthermore, single nuclei transcriptional data available for E110 in the Psychencode project (37) confirm that cortical neural progenitors expressing Pax6, Sox2, HOPX, and the glial precursor marker, EGFR, are gliogenic, whereas the only place where these markers clustered with neuronal progenitors was in the hippocampus, where neurogenesis is known to continue (*SI Appendix*, Fig. S1 *A–D*; data not available for Tbr2). (38, 39). Finally, we

Table 2. Percentage of Ki67+ cells expressing either Tbr2 or EGFR in the VZ/iSVZ, IFL, oSVZ, or IZ at E97.

	VZ	IFL	oSVZ	IZ
Tbr2+Ki67+/Ki67+	1.2	0	3.3	0
EGFR+Ki67+/Ki67+	63.5	87.1	60.0	82.7

counted Ki67+ proliferating cells in the VZ/iSVZ, inner fiber layer (IFL), oSVZ, and IZ (Fig. 3 *H* and *I*) and found that at E97, the majority of mitotic cells co-expressed EGFR and only a tiny fraction (1 to 3%) expressed a low level of Tbr2 (Table 2), reflecting the switch from neurogenesis to gliogenesis.

Acute (1 h survival) BrdU injection at E97 demonstrated large numbers of proliferative cells in the cortical wall, residing in the cortical plate (CP), SP, IZ, oSVZ, IFL, and VZ/SVZ (Fig. 3 *F* and *G*). The strong majority of the proliferative cells exiting the germinal zones into the IFL or IZ at this stage were EGFR+ glial precursors (Table 2) or likely endothelial cells lining blood vessels (Fig. 3*H*) (38). Thus, although neurogenesis ceases by about E90-100, the oSVZ generates large numbers of glial cells during the main gyrification period (38). Therefore, our data support neither a role for the oSVZ in the genesis of additional radial units specific to the superficial cortical layers beyond about E100 (the lissencephalic visual cortex excepted), nor a role for such neurons in the creation of gyral domes in the primate cerebrum.

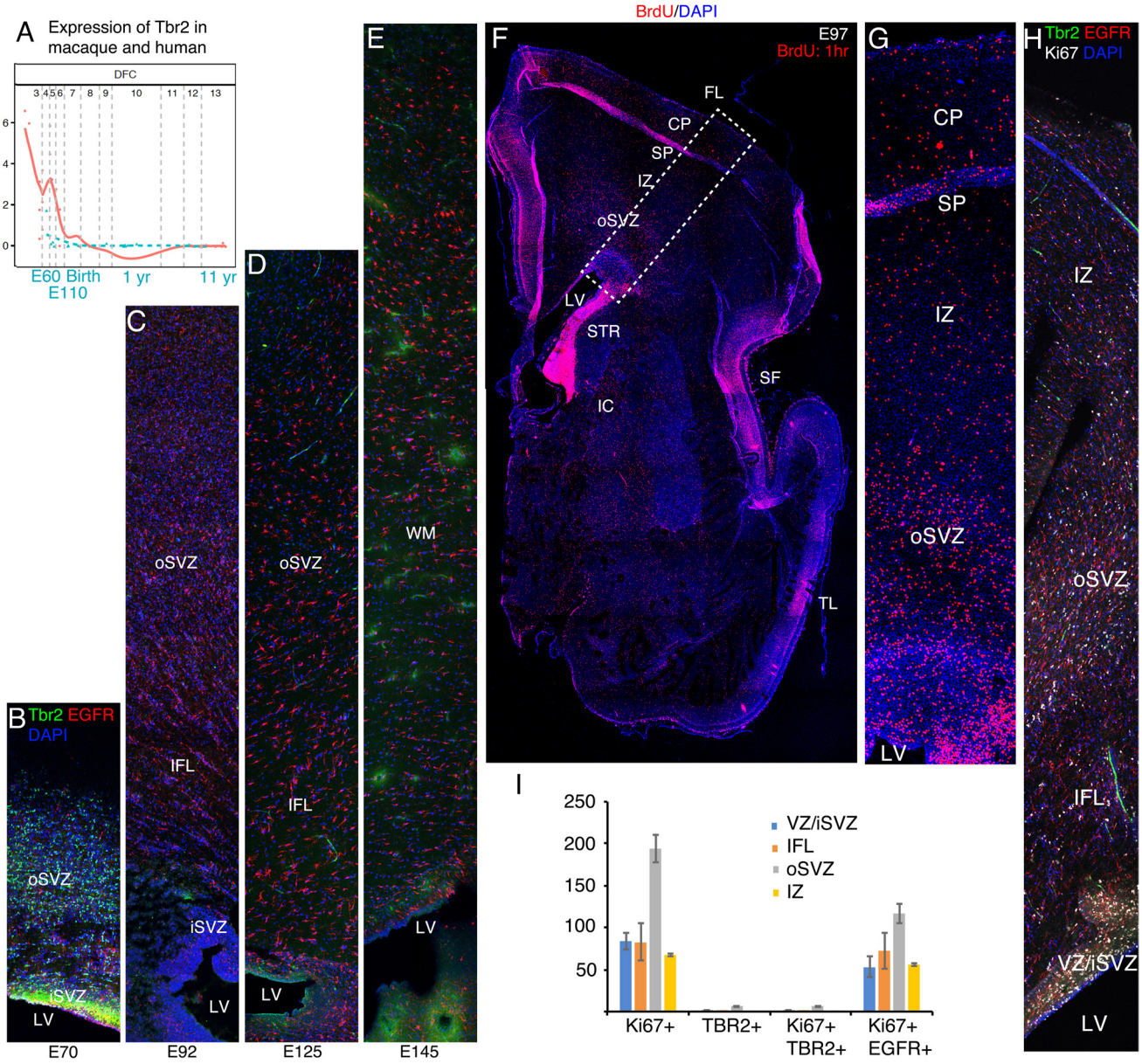

Fig. 3. Cessation of neurogenesis and transition to gliogenesis by E97. (*A*) Transcriptome analysis using the online Psychencode database (34) (http://evolution.psychencode.org/#) indicates loss of Tbr2 expression in dorsolateral prefrontal cortex (DFC) prior to E110 in macaque (blue line) and prior to the equivalent developmental stage in humans (red line). Y-axis represents normalized gene expression as log2(RPKM+1) where RPKM is number of reads per million kilobases. The vertical gray lines separate developmental stages: 3, early fetal; 4 to 6, mid fetal; 7, late fetal; 8 to 9, infancy; 10 to 11, childhood; 12, adolescence; 13 to 15, adulthood. The vertical gray line between 7 and 8 represents birth in both species as described (34). (*B–E*) Immunohistochemistry (IHC) for Tbr2 and EGFR in coronal macaque dorsal parietal brain sections at the indicated ages. By IHC, robust Tbr2 expression was found in the iSVZ and oSVZ at E70 (*B*), but only a few cells were found at E92 (*C*). Tbr2 expression was not detected at E125 or E145 (*D* and *E*). In contrast, EGFR expression continues in the iSVZ and oSVZ through E145. (*F*) Acute BrdU (1 h) labeling shows the position of cells in S phase in a whole cerebral hemisphere; boxed region magnified in (*G*). (*H*) E97 IHC showing triple labeling of Ki67, Tbr2, and EGFR and quantified in (*I*). Images are confocal montages. (Scale bar, 200 μm in (*B–E*), (*H*), 800 μm in (*F*).) Error bars represent SEM. FL, frontal lobe; IC, internal capsule; LV, lateral ventricle; SF, Sylvian fissure; STR, striatum; TL, temporal lobe.

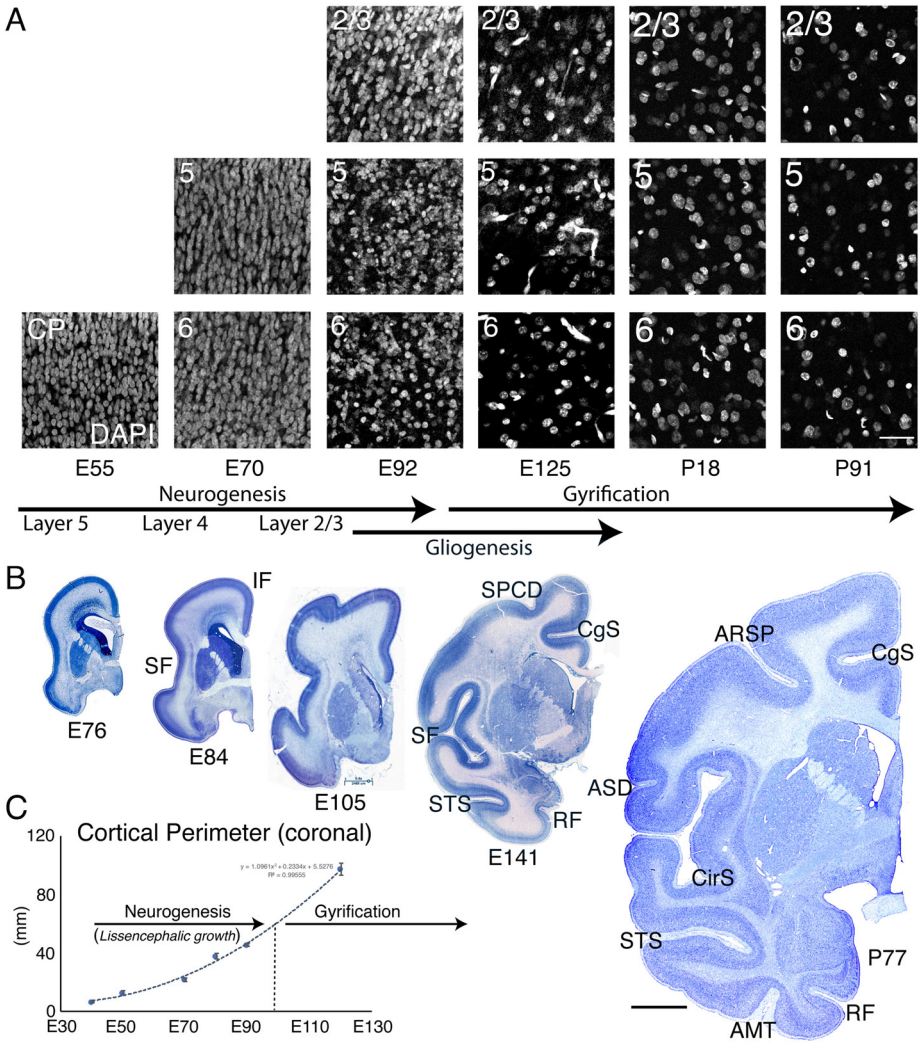

Fig. 4. Cortical plate surface expansion and gyrification due to neuropil production. The decrease in cellular density in different cortical laminae is indicated by DAPI staining in a series of coronal sections of dorsal parietal macaque cerebrum from E55-P91 (*A*). The decrease in cellular density becomes evident between E70 and E92, but dramatically accelerates between E92 and E125, just prior to initial cortical gyral development (*A–C*). (*B*) Coronal Nissl-stained macaque sections at the indicated ages showing dramatic cortical surface area growth, particularly after E90, at the completion of neurogenesis, which is explained largely by the massive decrease in neuronal density. (*C*) Coronal cortical perimeter measured from the corpus callosum to the lateroventral edge of the cortical plate at the level of the anterior commissure. Error bars represent SEM. Abbreviations: SPCD, superior precentral dimple; SF, Sylvian fissure; IF, interhemispheric fissure; CgS, cingulate sulcus; RF, rhinal fissure; ARSP, arcuate sulcus spur; ASD, anterior subcentral dimple; AMT, anterior middle temporal sulcus; CirS, circular sulcus; STS, superior temporal sulcus.(Scale bar in *A*, 40 μm; scale bar in B, 4 mm.)

Since localized neurogenesis of the oSVZ does not, and, based on timing alone, cannot explain the formation of cortical gyri, we focused on the growth of neuropil, which has been reported to be important in the surface expansion and gyrification of the cerebral cortex (6). We examined the rise of neuropil to precisely determine its relationship to the cessation of neurogenesis and onset of gyrification in macaque monkeys at E54, E55, E68, E70, E76, E84, E92, E97, E121, E125, E138, E141, E145, P18, P77, and P91. Between E55 and E70, cellular density in the cortical plate remains stable, while by E92 it decreases substantially (Figs. 4*A* and 5*A*). Between E92 and E125, we found the largest decrease in cellular density, due to the large increase in neuropil expressing β-III-tubulin and MAP2 (Figs. 4*A* and 5 *D* and *E* and *SI Appendix*, Fig. S2). Interestingly, this period corresponds to the initiation of gyral development in macaque. Analysis at P18 and P91 demonstrated continued decreased cellular density (Figs. 4*A* and 5*A*). Values for the percentage decline of DAPI-labeled nuclear density were E55→E70: +2.6%, E70→E92: −45.4%; E92→E125: −72.0%; E125→P18: +4.7%; P18→P91: −35.8% (Fig. 5*A*). Total DAPI density from E70 to P91 declined from 418.69 to 43 cells/160 μm × 160 μm image region, a decrease of 9.74-fold. When normalized for excitatory neuronal density (Fig. 5*B*), as assessed by combined Brn2/Ctip2/Tbr1 prior to E92 and NeuN thereafter, the values showed an even sharper decline: E55→E70: +3.3%, E70→E92: −48.2%; E92→E125: −76.0%; E125→P7: −20.8%; P7→P91: −42.0%. Total neuronal density from E70 to P91 declined by −94.3% or 17.5-fold. This accounts for the intercalation of other, principally glial, cell types originating substantially from HOPX+ gliogenic progenitors (Fig. 5 *F* and *G* and *SI Appendix*, Fig. S2*C*) (38). Accounting for interneurons moved further the decrease in excitatory neuron density to 95.7% percent or 23.4-fold by adulthood based on the reported 3:1 ratio of excitatory to inhibitory neurons in macaque (40). Remarkably, the cortical perimeter of coronal sections at the level of the anterior commissure showed more rapid growth in the post-neurogenic period than during neurogenesis, reflecting the massive, rapid neuropil growth (Fig. 4 *B* and *C*). Note that the increase in perimeter of the superficial layers was approximately equal to that of the deep layers (Figs. 2*A* and 4*B*). Thus, the peak of the cortical neuropil explosion coincides with the peak of early gyral development, and intracortical neuropil growth

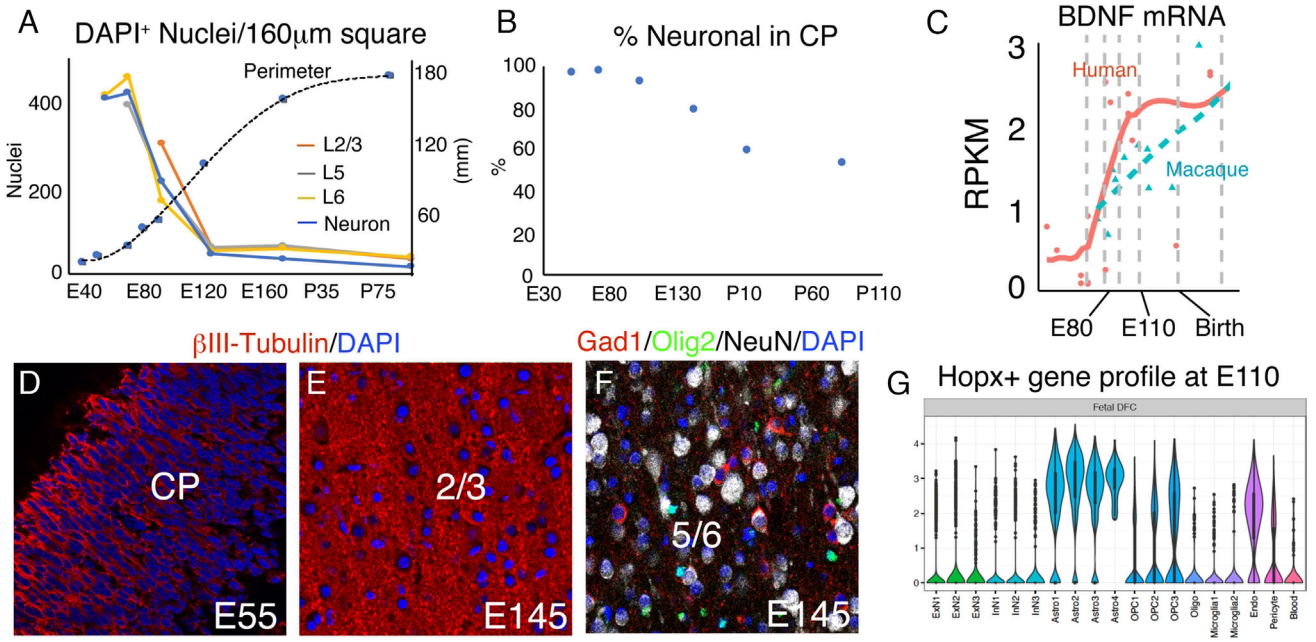

Fig. 5. Neuropil growth, regulation, and cell-type diversification in the developing macaque cortical plate. (*A*) DAPI nuclear density in 160 μm square regions of single confocal images, by cortical layer as shown in Fig. 4*A*, with neuronal density plotted in blue. (*B*) Percentage of total DAPI-labeled nuclei that stain for neuronal markers; Tbr1 at E55, Tbr1/Ctip2/Brn2 at E70-E97, and NeuN at E145, P7, and P91. Neuronal density declines faster than cellular density after E70. (*C*) Single-cell transcriptome data via Psychencode showing that humans express higher levels of BDNF in dorsal frontal cortex than do macaques during gyrification. (*D* and *E*) Neuropil labeled by βIII-tubulin IHC. (*F*) Neurons, OPCs, and interneurons revealed by NeuN, Olig2, and Gad1, respectively. (*G*) Psychencode data showing that Hopx+ cells express gene clusters principally associated with astrocyte and OPC lineages at E110. [Scale bar: 40 μm in (*D*–*F*).]

continues to represent a strong mechanical expansion force as gyri grow, until at least the third postnatal month.

Since BDNF was associated with increased neuropil in both humans and rodents (31, 32), we examined its distribution in developing monkey neocortex. Previous studies have shown a sustained increase in BDNF mRNA expression during macaque development from embryonic stages to adult (41). Fig. 6 shows that indeed BDNF protein is highly expressed in cortical neurons by E70 and by E145, BDNF is clearly expressed in astrocytes in the cortex, but not in the underlying IZ (Fig. 6). Thus, we suggest that neurotrophin-driven neuropil growth is likely to feature prominently in cortical gray matter expansion and gyrification in evolution and disease (35).

Discussion

While an increased number of radial units are critical for cerebral surface area growth across mammals (1), gyrencephalic mammals also possess genetic instructions that tend to increase neuron and glial size and intracortical neuropil volume and complexity, which, in turn, amplifies surface area expansion. Our data indicate that much of the cortical surface area expansion in macaque is in fact accomplished in the post-neurogenic period coincident with the rapid growth of intracortical neuropil, and it is likely that, since humans have an even lower neuronal density than macaque (40), neuropil growth represents an even more important source of cortical growth in homo sapiens (37).

Our data demonstrate that intracortical neuropil expansion and gliogenesis together lead to a 23.4-fold decrease in overall cortical plate excitatory neuronal density from E70 to P91, and the rate of cortical expansion reaches its maximum in the post-neurogenic period. Using MRI during fetal development, a 7.2-fold increase (from 8.2 to 59 cm^2) in neocortical surface area between E75 and E138 has been reported (29). Our data for the same period reflect a 4.5-fold increase in the perimeter of the neocortex. Interestingly, consistent with our data, the same study (29) also found that the rate of surface area increase accelerates after E102, when neurogenesis is already finished (31–33). While our data rely on cross sections rather than 3D volumetric analysis, our data are consistent with these other reports and indicate that the magnitude of neuropil-driven surface area expansion far exceeds any contribution of the arrival of the final few migrating excitatory neurons occurring around E100; indeed radial neuronal migration is complete in some cortical areas by E80 (3).

Across mammalian species, the amount of neuropil in cortical gray matter typically increases with cerebral gyrification. For example, it is reported that cortical neuronal density (including both excitatory and inhibitory) in humans is lower (~15,000 to 24,000 neurons/mm^3) than that of macaque (~73,000 neurons/mm^3) and that of rodents (rat: 54,000 neurons/mm^3; mouse: 120,000 neurons/mm^3) (40, 42), while the cetacean brain shows a neuronal density of 7,000 to 16,000 neurons/mm^3 and some of the highest gyrification indices, also in part due to thinner cortices (43, 44). Within species, the primary visual cortex of macaque is nearly lissencephalic, and neuronal density there (143,000 neurons/mm^3) is greater than other cortical regions and even higher than that of mouse (42). The evolutionary increase in cellular volume is not limited to neurons, as human astrocytes also are reported to have 16.5-fold greater volume than those of mice (45). Therefore, both across species and across brain regions, an increased gyrification index is typically correlated with increased cortical neuropil production.

The marmoset, a new world monkey with a neuronal density of 80,000 neurons/mm^3 (46) and a well-developed oSVZ with abundant oRG (19), exhibits a lissencephalic brain. Therefore, as noted previously (6, 7), an increase in the amount of neuropil per neuron, particularly when combined with thin cortices, typically accompanies an increase in gyrification regardless of overall size, and the presence of a robust oSVZ does not necessarily lead to gyrification (18). However, while our data indicate that lateral

surface area expansion due to direct insertion of new neurons via localized neurogenesis does not account for gyrification in macaque, the present data cannot rule out that possibility in other mammalian species such as ferret (47).

Studies of gyrification in humans lack precise experimental methods to detect dividing cells, including BrdU or ^{3}TdR labeling, and therefore, the timing of neurogenesis can only be estimated based on postmortem immunohistochemistry studies (48). This underscores the importance of research in non-human primates, where ^{3}TdR and BrdU studies have allowed a precise determination of the timing of the cessation of neurogenesis (31). Here we correlated the precise end of neurogenesis in macaque with the disappearance of Tbr2 expression, indicating that the cessation of neurogenesis can be inferred by the disappearance of Tbr2 in human fetal development. Thus, non-human primates remain a very useful model of human development, far exceeding other gyrencephalic species with different cortical configurations such as carnivores, e.g., with the ability to model secondary gyri. We do not expect the overall mechanisms of gyrification to differ substantially between macaque and human.

We hypothesized that genes controlling neuropil growth, such as neurotrophins and their receptors, could also feature prominently in the evolution of gyrencephaly. BDNF has been associated with pathological states in human leading to megalencephaly and cases of autism spectrum disorders where large brains and hyperproduction of neuropil are observed (49). Furthermore, experiments in rodents have demonstrated that loss of BDNF causes increased neuronal density and reduced neuropil, with consequent thinning of the cortex and reduced surface area due to lack of maturation and maintenance of cortical dendrites (50). We speculate that human mutations in BDNF, its receptor, TrkB, or other neuropil growth genes could lead to microcephaly characterized by increased cortical neuron density and consequent gyrification abnormalities. The individual neuropil maturation and growth rates within each cortical area and indeed each layer during development remain unknown, but it is plausible that they differ in a manner consistent with the differential tangential expansion hypothesis (20, 51). However, the main difference, we propose, is that these forces are maturational in nature and not produced by direct insertion of new neurons and they do not disrupt radial columns. We suggest that the patterned genesis of different classes of neurons and glia within the VZ and SVZ of each cortical proto-area could lead to locally different postmigratory volumetric growth of neuropil and hence influence gyral development and pattern.

Another factor contributing to the large increase in neuropil is the arrival of large numbers of cortico-thalamic and cortico-cortical axons. Indeed, spatiotemporal asymmetry in the outgrowth and cortical invasion of those afferents might also contribute to create the pattern of gyri and sulci characteristic of a given species (10), and indeed gyral patterns can be changed by the surgical manipulation of axonal pathways during the post-neurogenic period in non-human primates (1). Increased gray matter volume due to neuropil growth would be expected to increase cortical thickness to some degree, which likely would constrain the curvature of any cortical fold as noted previously (6, 52, 53); thus the factors that constrain cortical thickness and its relation to the malleability of the cortical surface should be further examined with respect to the number of neurons in each layer and the geometry of the neuropil growth. The role of radial anisotropy in the cortex (e.g., by tension exerted by apical dendrites of pyramidal neurons) might be a factor limiting the radial growth (thickness) of the cortex, in contrast to less restrained tangential expansion (surface area), as recently highlighted by Van Essen (54, 55). Finally, monozygotic twins do not have precisely the same gyral patterns and sulcal depths, but it is reported that the variance is less than in dizygotic twins (56), suggesting that genetic factors contribute to basic gyral characteristics. Thus, we speculate that the remaining variance is driven by stochastic mechanisms like a fingerprint and is of greater magnitude with tertiary and some secondary gyri, while the more primitive gyri are more conserved. The sum of these factors thus sets the stage for the maturational properties of a given region or species of mammalian cortex.

The protomap and radial unit model of cortical development is thus supported by the most advanced genetic methods (57) and can be extended to the principle of gyrification via these maturational characteristics. We suggest that the evolutionary genetics of massive, rapid neuropil growth should be explored across cortical areas with neurotrophic factor pathways in the context of brain malformations such as microcephaly, macrocephaly, lissencephaly, and cognitive developmental syndromes with such structural correlates (57).

In conclusion, our data indicate that massive, rapid intracortical neuropil growth is a principal driving factor for the formation of primate cortical convolutions. A variety of additional mechanical factors including the addition of glial cells to the cortical plate, the arrival and integration of thalamocortical and cortico-cortical afferents, and the patterned expansion of large cerebral axonal tracts in the underlying white matter (58) can be concluded to drive the process of cerebral gyrification, which is ultimately predicated upon the expansion of radial units originating from the VZ. Areal differences in neuropil growth could occur and may be a product of the maturation characteristics (e.g., total volume) of the particular varieties of resident cortical neurons and glia, which in turn would be expected to contribute to the pattern of gyral formation. Reproduction of the basic gyral pattern of primary, and the initial development of secondary gyri, across individuals is therefore likely to be genetically encoded within the cortical protomap and as a function of the afferent inputs with which the early cortex interacts. It should be noted within this classical framework that, as previously reported (6), other factors such as local cortical thickness and physical barriers including other gyri also constrain the growth and shape of cortical convolutions. Thus, the summation and relative contribution of all these factors may differ in timing and importance for the development of each convolution along the cortical surface.

Materials and Methods

Animals and Tissue Processing. Animal studies were performed in accordance with Yale Institutional Animal Care and Use Committee guidelines. Animal breeding, timing of pregnancies, and collection of fetal brains by caesarian section have previously been described (59). A total of 21 timed-pregnant fetal and postnatal macaque monkey brains were produced in-house at the Yale Animal Resource Center, including the following ages: E54, E55, E68, E70, E76, E84, E92, E97, E121, E125, E130, E138, E141, E145, P18, P77, P91, and 3× 3 y. Prenatal brains were collected and immerse-fixed in 4% paraformaldehyde overnight, washed in PBS and equilibrated in 30% sucrose/PBS for up to 3 d, and processed into freeze blocks (38). Coronal blocks representing parietal or frontal cerebral cortex were cryosectioned at 25 μm and placed on Superfrost Plus slides (VWR), dried overnight at room temperature, and the slides subsequently frozen at −20°C until staining. Some brains using surgical resection are part of the existing MacBrainResource, and no additional animals were sacrificed for those data.

Immunohistochemistry and BrdU Labeling. Fluorescence immunohistochemistry utilized a citrate-based antigen retrieval step involving pH 6.0 sodium citrate in water heated to 95 °C for 7 min, followed by cooling to room temperature and immunostained as described previously (38). Antibodies and dilutions are as follows: rabbit anti-Pax6 (Millipore; 1:750), rabbit Hopx (Sigma; 1:500); mouse anti-Ki67 (Vector; 1:300), goat anti-EGFR (R&D Systems; 10 mg/mL);

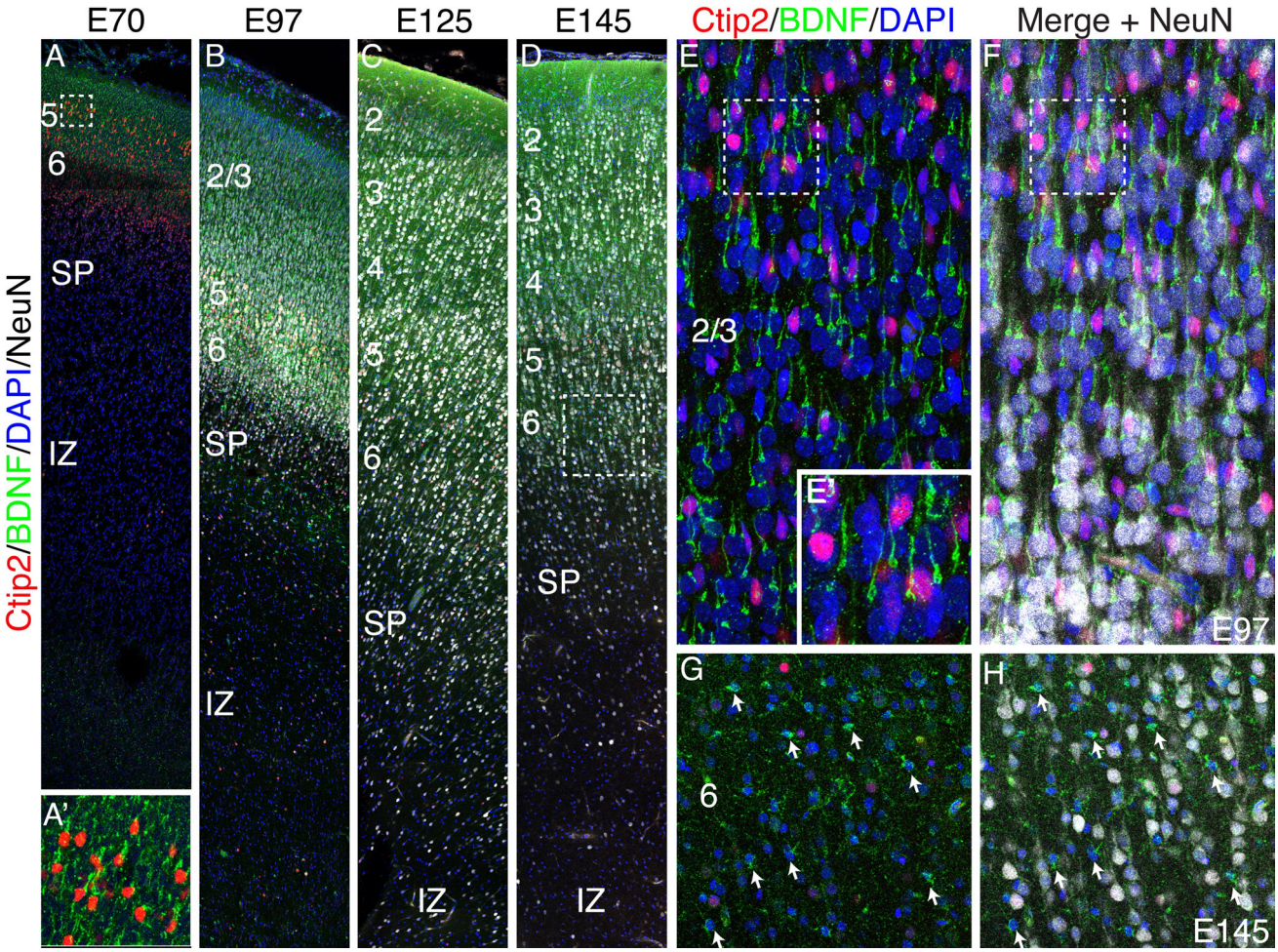

Fig. 6. Enriched BDNF expression in macaque cortical neurons and glia during gyrification. (*A*–*D*) Series of coronal sections of macaque dorsal frontal cortex from E70-E145 stained for Ctip2, BDNF, NeuN, and DAPI. At all ages examined, BDNF was highly expressed in the apical dendrite of excitatory cortical neurons and enriched in Ctip2+ layer five neurons. (*A*–*F*, *A'*). (*E* and *F*) High magnification confocal Z-stack of cortical neurons at E97. (*E'*) Magnified image of the boxed region in (*E*). (*F*) NeuN labels almost all cortical cells at E97. (*G* and *H*) However, by E145 many cells are NeuN-negative putative glia, displaying diminutive somal size, and multipolar or stellate morphology, most of which express high levels of BDNF.

rabbit anti-Olig2 (Abcam; 1:2,000), rabbit anti-Tbr1 (Abcam; 1:1,000), rat anti-GFAP (1:100), mouse anti-βIII-tubulin (R&D Systems; 1:1,000), chicken anti-Tbr2 (Millipore; 1:200), rat anti-BrdU (Accurate Chemical; 1:400); secondary antibodies and dilutions were donkey anti-goat/chicken/rat, 1:1,000, DyLight 488/543/647 (Jackson Laboratories). Blocking utilized reconstituted Donkey Serum. Sections were counterstained with DAPI mounting medium (Vector) to label cellular nuclei. A single injection of BrdU at 50 mg/kg (Sigma; in 0.9% NaCl with 0.007 N NaOH) was delivered intravenously at E97, with sacrifice 1 h later.

Imaging and Image Processing. Confocal imaging was performed on a Zeiss LSM 510 confocal microscope with a Coherent Chameleon titanium sapphire 2-photon laser (38) and 488 argon and 543 and 633 nm HeNe laser lines. The 2-photon laser was set at 720 nm to excite DAPI. Z-stacks were acquired at either 20X (0.8NA) or 40X (1.1NA) resolution and one airy unit optical section thickness. XYZ tile scans representing montage images were acquired in Zen (Zeiss). Images were processed to max projections in FIJI and then into figures in Adobe Photoshop and Illustrator CS5. Neuronal and DAPI density measurements were done using 160 μm square image regions from confocal images representing identical tissue volumes across embryonic timepoints. Ki67, Tbr2, EGFR and double labeled cells were counted using the cell counter tool in FIJI (NIH) using a single optical section corresponding to an optical section depth of 2.8 μm. Three radial columns 185 μm wide were used for counting at E97; means are reported with SEM. Nissl sections were imaged using a Leica Aperio CS2 slide scanner. Cortical perimeter measurements from the corpus callosum to the ventrolateral edge of the cortical plate at the level of the anterior commissure were done in ImageJ utilizing images from the MacBrain Resource Center (https://medicine.yale.edu/neuroscience/macbrain/) and Allen Brain Atlas. Error bars represent SEM, and best fit line for cortical perimeter was a polynomial equation generated by Microsoft Excel.

Data, Materials, and Software Availability. All study data are included in the article and/or *SI Appendix*.

ACKNOWLEDGMENTS. We thank the MacBrain Resource Center (supported by MH113257 to A.D.) for providing materials for this investigation and Mariamma Pappy for lab help including the restoration of Nissl-stained macaque brain sections. We are grateful to the Kavli Institute for Neuroscience at Yale and the NIH grant DA023999 to P.R.

Author affiliations: [a]Department of Neuroscience, Yale University, New Haven, CT 06520; and [b]Kavli Institute for Neuroscience at Yale, Yale University, New Haven, CT 06520

1. P. Rakic, Specification of cerebral cortical areas. *Science* **241**, 170–176 (1988).
2. P. Rakic, Evolution of the neocortex: A perspective from developmental biology. *Nat. Rev. Neurosci.* **10**, 724–735 (2009).
3. P. Rakic, A small step for the cell, a giant leap for mankind: A hypothesis of neocortical expansion during evolution. *Trends Neurosci.* **18**, 383–388 (1995).
4. C. Dehay, H. Kennedy, Cell-cycle control and cortical development. *Nat. Rev. Neurosci.* **8**, 438–450 (2007).

5. S. C. Noctor, A. C. Flint, T. A. Weissman, R. S. Dammerman, A. R. Kriegstein, Neurons derived from radial glial cells establish radial units in neocortex. *Nature* **409**, 714–720 (2001).
6. W. Welker "Why does cerebral cortex fissure and fold?" in *Cerebral Cortex*,A. Peters, E. G. Jones, Ed. (1990), New York: Plenum Press, **vol. 8B**, pp. 3–136.
7. M. Jacobson, Developmental Neurobiology (Springer, Boston, MA, ed. Third, 1991).
8. E. Armstrong, A. Schleicher, H. Omran, M. Curtis, K. Zilles, The ontogeny of human gyrification. *Cereb. Cortex* **5**, 56–63 (1995).
9. D. P. Richman, R. M. Stewart, J. W. Hutchinson, V. S. Caviness Jr., Mechanical model of brain convolutional development. *Science* **189**, 18–21 (1975).
10. D. C. Van Essen, A tension-based theory of morphogenesis and compact wiring in the central nervous system. *Nature* **385**, 313–318 (1997).
11. I. Kostovic, P. Rakic, Developmental history of the transient subplate zone in the visual and somatosensory cortex of the macaque monkey and human brain. *J. Comp. Neurol.* **297**, 441–470 (1990).
12. P. Rakic, J. P. Bourgeois, P. S. Goldman-Rakic, Synaptic development of the cerebral cortex: Implications for learning, memory, and mental illness. *Prog. Brain Res.* **102**, 227–243 (1994).
13. A. Kriegstein, S. Noctor, V. Martinez-Cerdeno, Patterns of neural stem and progenitor cell division may underlie evolutionary cortical expansion. *Nat. Rev. Neurosci.* **7**, 883–890 (2006).
14. I. Reillo, C. de Juan Romero, M. A. Garcia-Cabezas, V. Borrell, A role for intermediate radial glia in the tangential expansion of the mammalian cerebral cortex. *Cereb. Cortex* **21**, 1674–1694 (2011).
15. E. Lewitus, I. Kelava, W. B. Huttner, Conical expansion of the outer subventricular zone and the role of neocortical folding in evolution and development. *Front. Hum. Neurosci.* **7**, 424 (2013).
16. R. Stahl *et al.*, Trnp1 regulates expansion and folding of the mammalian cerebral cortex by control of radial glial fate. *Cell* **153**, 535–549 (2013).
17. L. Del-Valle-Anton, V. Borrell, Folding brains: From development to disease modeling. *Physiol. Rev.* **102**, 511–550 (2022).
18. R. F. Hevner, T. F. Haydar, The (not necessarily) convoluted role of basal radial glia in cortical neurogenesis. *Cereb. Cortex* **22**, 465–468 (2012).
19. I. Kelava *et al.*, Abundant occurrence of basal radial glia in the subventricular zone of embryonic neocortex of a lissencephalic primate, the common marmoset Callithrix jacchus. *Cereb. Cortex* **22**, 469–481 (2012).
20. C. D. Kroenke, P. V. Bayly, How forces fold the cerebral cortex. *J. Neurosci.* **38**, 767–775 (2018).
21. C. Dehay, H. Kennedy, K. S. Kosik, The outer subventricular zone and primate-specific cortical complexification. *Neuron* **85**, 683–694 (2015).
22. V. Martinez-Cerdeno *et al.*, Comparative analysis of the subventricular zone in rat, ferret and macaque: Evidence for an outer subventricular zone in rodents. *PloS One* **7**, e30178 (2012).
23. K. Fukunishi *et al.*, Development of cerebral sulci and gyri in fetuses of cynomolgus monkeys (Macaca fascicularis). *Anat. Embryol. (Berl)* **211**, 757–764 (2006).
24. K. Fukunishi *et al.*, Correlation between formation of the calcarine sulcus and morphological maturation of the lateral ventricle in cynomolgus monkey fetuses. *Acta Neurobiol. Exp. (Wars)* **71**, 381–386 (2011).
25. K. Sawada *et al.*, Developments of sulcal pattern and subcortical structures of the forebrain in cynomolgus monkey fetuses: 7-tesla magnetic resonance imaging provides high reproducibility of gross structural changes. *Brain Struct. Funct.* **213**, 469–480 (2009).
26. K. Sawada *et al.*, Neuroanatomic and magnetic resonance imaging references for normal development of cerebral sulci of laboratory primate, cynomolgus monkeys (Macaca fascicularis). *Congenit. Anom. (Kyoto)* **52**, 16–27 (2012).
27. K. Sakamoto *et al.*, Postnatal change in sulcal length asymmetry in cerebrum of cynomolgus monkeys (Macaca fascicularis). *Anat. Rec. (Hoboken)* **297**, 200–207 (2014).
28. M. Kashima *et al.*, Development of cerebral sulci and gyri in fetuses of cynomolgus monkeys (Macaca fascicularis). II. Gross observation of the medial surface. *Brain Struct. Funct.* **212**, 513–520 (2008).
29. X. Wang *et al.*, Folding, but not surface area expansion, is associated with cellular morphological maturation in the fetal cerebral cortex. *J. Neurosci.* **37**, 1971–1983 (2017).
30. G. C. Ribas, The cerebral sulci and gyri. *Neurosurg. Focus* **28**, E2 (2010).
31. P. Rakic, Neurons in rhesus monkey visual cortex: Systematic relation between time of origin and eventual disposition. *Science* **183**, 425–427 (1974).
32. B. Granger, F. Tekaia, A. M. Le Sourd, P. Rakic, J. P. Bourgeois, Tempo of neurogenesis and synaptogenesis in the primate cingulate mesocortex: Comparison with the neocortex. *J. Comp. Neurol.* **360**, 363–376 (1995).
33. P. Rakic, Neurogenesis in adult primate neocortex: An evaluation of the evidence. *Nat. Rev. Neurosci.* **3**, 65–71 (2002).
34. Y. Zhu *et al.*, Spatiotemporal transcriptomic divergence across human and macaque brain development. *Science* **362**, eaat8077 (2018).
35. C. Englund *et al.*, Pax6, Tbr2, and Tbr1 are expressed sequentially by radial glia, intermediate progenitor cells, and postmitotic neurons in developing neocortex. *J. Neurosci.* **25**, 247–251 (2005).
36. S. C. Noctor, V. Martinez-Cerdeno, L. Ivic, A. R. Kriegstein, Cortical neurons arise in symmetric and asymmetric division zones and migrate through specific phases. *Nat. Neurosci.* **7**, 136–144 (2004).
37. A. M. M. Sousa *et al.*, Molecular and cellular reorganization of neural circuits in the human lineage. *Science* **358**, 1027–1032 (2017).
38. B. G. Rash *et al.*, Gliogenesis in the outer subventricular zone promotes enlargement and gyrification of the primate cerebrum. *Proc. Natl. Acad. Sci. U.S.A.* **116**, 7089–7094 (2019).
39. W. Huang *et al.*, Origins and proliferative states of human oligodendrocyte precursor cells. *Cell* **182**, 594–608.e511 (2020).
40. J. DeFelipe, L. Alonso-Nanclares, J. I. Arellano, Microstructure of the neocortex: Comparative aspects. *J. Neurocytol.* **31**, 299–316 (2002).
41. T. Mori, K. Takumi, K. Shimizu, T. Oishi, M. Hayashi, Heterogeneity of the developmental patterns of neurotrophin protein levels among neocortical areas of macaque monkeys. *Exp. Brain Res.* **171**, 129–138 (2006).
42. J. R. Christensen *et al.*, Neocortical and hippocampal neuron and glial cell numbers in the rhesus monkey. *Anat Rec. (Hoboken)* **290**, 330–340 (2007).
43. S. H. Ridgway, R. H. Brownson, K. R. Van Alstyne, R. A. Hauser, Higher neuron densities in the cerebral cortex and larger cerebellums may limit dive times of delphinids compared to deep-diving toothed whales. *PLoS One* **14**, e0226206 (2019).
44. D. B. Tower, Structural and functional organization of mammalian cerebral cortex; the correlation of neurone density with brain size; cortical neurone density in the fin whale (Balaenoptera physalus L.) with a note on the cortical neurone density in the Indian elephant. *J. Comp. Neurol.* **101**, 19–51 (1954).
45. N. A. Oberheim *et al.*, Uniquely hominid features of adult human astrocytes. *J. Neurosci.* **29**, 3276–3287 (2009).
46. N. Atapour *et al.*, Neuronal distribution across the cerebral cortex of the marmoset monkey (Callithrix Jacchus). *Cereb. Cortex* **29**, 3836–3863 (2019).
47. V. Borrell, How cells fold the cerebral cortex. *J. Neurosci* **38**, 776–783 (2018).
48. S. Malik *et al.*, Neurogenesis continues in the third trimester of pregnancy and is suppressed by premature birth. *J. Neurosci.* **33**, 411–423 (2013).
49. J. Y. Koh, J. S. Lim, H. R. Byun, M. H. Yoo, Abnormalities in the zinc-metalloprotease-BDNF axis may contribute to megalencephaly and cortical hyperconnectivity in young autism spectrum disorder patients. *Mol. Brain* **7**, 64 (2014).
50. J. A. Gorski, S. R. Zeiler, S. Tamowski, K. R. Jones, Brain-derived neurotrophic factor is required for the maintenance of cortical dendrites. *J. Neurosci.* **23**, 6856–6865 (2003).
51. L. Ronan, P. C. Fletcher, From genes to folds: A review of cortical gyrification theory. *Brain Struct. Funct.* **220**, 2475–2483 (2015).
52. B. Mota, S. Herculano-Houzel, BRAIN STRUCTURE. Cortical folding scales universally with surface area and thickness, not number of neurons. *Science* **349**, 74–77 (2015).
53. D. C. Van Essen *et al.*, Cerebral cortical folding, parcellation, and connectivity in humans, nonhuman primates, and mice. *Proc. Natl. Acad. Sci. U.S.A.* **116**, 26173–26180 (2019), 10.1073/pnas.1902299116.
54. D. Van Essen, A 2020 view of tension-based cortical morphogenesis. *Proc. Natl. Acad. Sci. U.S.A.* **117**, 12 (2020).
55. D. Van Essen, Biomechanical models and mechanisms of cellular morphogenesis and cerebral cortical expansion and folding. *Semin. Cell Dev. Biol.* (2022), in press.
56. D. Duan *et al.*, Individual identification and individual variability analysis based on cortical folding features in developing infant singletons and twins. *Hum. Brain Mapp.* **41**, 1985–2003 (2020).
57. B. I. Bae *et al.*, Evolutionarily dynamic alternative splicing of GPR56 regulates regional cerebral cortical patterning. *Science* **343**, 764–768 (2014).
58. Y. Shinmyo *et al.*, Localized astrogenesis regulates gyrification of the cerebral cortex. *Sci. Adv.* **8**, eabi5209 (2022).
59. D. R. Kornack, P. Rakic, Changes in cell-cycle kinetics during the development and evolution of primate neocortex. *Proc. Natl. Acad. Sci. U.S.A.* **95**, 1242–1246 (1998).